CHAPTER 6 *Applications to problems with experimental response*

6.1 Introduction

This chapter applies the genetic programming methodology to building an analytical model using data collected from physical experiments. Optimization of an engineering system when only experimental response is available is of considerable importance in many applications.

Building an analytical model helps deeper understanding of a system or process under consideration. It also allows to improve its performance characteristics.

Three applications are presented: the approximation of design charts, the prediction of the shear strength in reinforced concrete deep beams and the multicriteria optimization of Roman cement.

6.2 Approximation of design charts for software development

6.2.1 Introduction

The design procedure for steel frame structures according to BS 5950 includes stability analysis. Generally, it is assumed that the structure as a whole will remain stable, from the commencement of erection until demolition. If the erected members are incapable of keeping themselves in equilibrium, then sufficient external bracing has to be provided for stability. The effect of instability has been reflected in the design process by determining the effective length of columns which, in essence, is equivalent to carrying out a stability analysis for every segment of a frame (Mahfouz, 1999).

BS 5950: Part1 differentiates between sway and non-sway frames based on the horizontal deflection of each storey. Using two restraint coefficients k_1 and k_2, the value of the effective length factor L_X^{eff} / L may be interpolated from plotted contour lines given in Figure 23 of BS 5950 in the case of a column in non-sway framework or Figure 24 of BS 5950 in the case of a column in sway framework. However, the code of practice does not provide any method to obtain these values analytically.

To incorporate the determination of the effective length factor for a column in either sway or non-sway framework into a computer based algorithm for steelwork design (Mahfouz,1999), genetic programming has been used to construct analytical expressions of the corresponding charts.

6.2.2 Experiments

The data used for training and validating the model have been directly read from Figures 23 and 24 in BS 5950. The figures are symmetrical on each side of the diagonal, so only the reading of half of the data is required. Each axis k_1 and k_2 has been divided into 100 equal divisions, resulting in $(101)^2 = 10201$ points. In the case of sway frames, response values L_X^{eff} / L greater than 5 are not plotted because they tend to infinity. Figure 6.1 shows surface plots for both sway and non-sway frames.

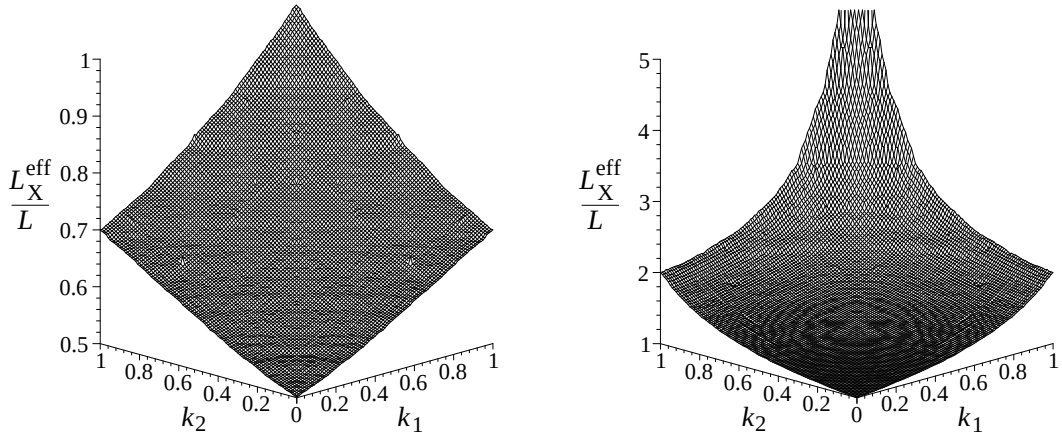

Figure 6.1 Surface plot of L_X^{eff} / L for a column in a rigid-jointed frame

For the training data, a subset of points corresponding to 20 divisions equally spaced on each axis has been selected. The plan of experiments contains $21^2 = 421$ points. The remaining 9780 points are used as validation data.

6.2.3 GP response

The model building in this application is a two step process. First, the analysis of the best individuals obtained in several runs of GP has suggested the type of polynomial

to be used. A typical expression in the case of columns in non-sway framework for one run is as follows:

$$L_X^{eff} / L = 0.5 + 0.14\ k_1 + 0.17\ k_2 + 0.092\ k_1^2 + 0.036\ k_2^2 - 0.12\ k_1\ k_2 + 0.34\ k_1^2\ k2 + 0.17\ k_1\ k_2^2 - 0.031\ k_1^4 - 0.32\ k_1^3\ k_2 - 0.22\ k_1^2\ k_2^2 + 0.13\ k_1^3\ k_2^2 + 0.14\ k_1^4\ k_2 \quad (6.1)$$

After careful comparison of the common terms of the best individuals in several runs, a general structure for the expression has been assumed. The second step has identified the tuning parameters that best fit the model into the training data. A nonlinear optimization technique (Madsen and Hegelund, 1991) has been applied to the following polynomial to find the coefficients:

$$\tilde{F}(k_1, k_2) = a_0 + \sum_{i=1}^{m} a_{1i} (k_1)^i + \sum_{i=1}^{m} a_{2i} (k_2)^i + \sum_{i=2}^{m} \sum_{j=1}^{i-1} a_{3ij} (k_1)^j (k_2)^{i-j} \quad (6.2)$$

where m is the order of the polynomial.

Several orders have been tested for non-sway framework, the best fit resulting in the following 4th order polynomial:

$$L_X^{eff} / L = 0.032573\ k_1^4 + 0.032573\ k_2^4 + 0.053264\ k_1^3\ k_2 - 0.032727\ k_1^2\ k_2^2 + 0.053264\ k_1\ k_2^3 - 0.134354\ k_1^3 - 0.134354\ k_2^3 + 0.015353\ k_1^2\ k_2 + 0.015353\ k_1\ k_2^2 + 0.185810\ k_1^2 + 0.185810\ k_2^2 - 0.000581\ k_1\ k_2 + 0.112912\ k_1 + 0.112912\ k_2 + 0.501496 \quad (6.3)$$

The RMS error of expression (6.3) over the validation data is 0.011. This error is acceptable taking into account the experimental error when reading the values from the chart. Figure 6.2 represents the expression (6.3).

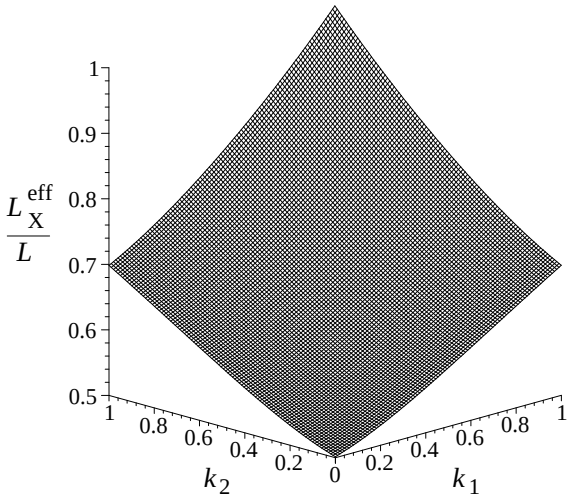

(a) Surface plot

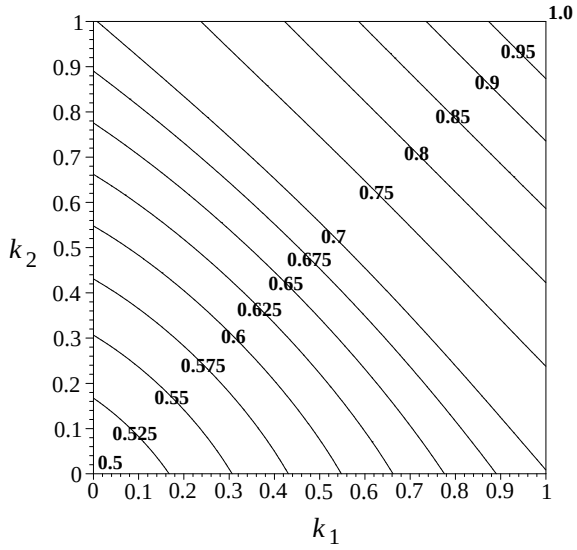

(b) Contour plot

Figure 6.2 Graphical representation of the 4th order polynomial of L_X^{eff} / L for a column in a rigid-jointed non-sway frame

For sway framework, the same methodology has come up with a 7^{th} order polynomial as follows:

$$L_X^{eff}/L = - 2.097553\ k_2^7 - 2.097552\ k_1^7 + 28.466829\ k_1^6\ k_2 + 51.483168\ k_1^5\ k_2^2 + 55.208934\ k_1^4\ k_2^3 + 55.208934\ k_1^3\ k_2^4 + 51.483168\ k_1^2\ k_2^5 + 28.466829\ k_1\ k_2^6 - 1.189593\ k_2^6 - 1.189593\ k_1^6 - 116.544967\ k_1^5\ k_2 - 176.815809\ k_1^4\ k_2^2 - 183.906621\ k_1^3\ k_2^3 - 176.815809\ k_1^2\ k_2^4 - 116.544967\ k_1 k_2^5 + 19.991420\ k_1^5 + 19.991419\ k_2^5 + 187.034054\ k_1^4\ k_2 + 244.951121\ k_1^3\ k_2^2 + 244.951121\ k_1^2\ k_2^3 + 187.034054\ k_1\ k_2^4 - 32.628183\ k_2^4 - 32.628183\ k_1^4 - 149.785571\ k_1^3\ k_2 - 173.496623\ k_1^2\ k_2^2 - 149.785571\ k_1\ k_2^3 + 22.725113\ k_2^3 + 22.725113\ k_1^3 + 63.487658\ k_1\ k_2^2 + 63.487658\ k_1^2\ k_2 - 7.034584\ k_2^2 - 7.034584\ k_1^2 - 13.689820\ k_1\ k_2 + 1.282744\ k_2 + 1.282744\ k_1 + 0.956325 \quad (6.4)$$

The RMS error of expression (6.4) over the validation data is 0.0097. Figure 6.3 shows the surface plot and the contour plot of expression (6.4).

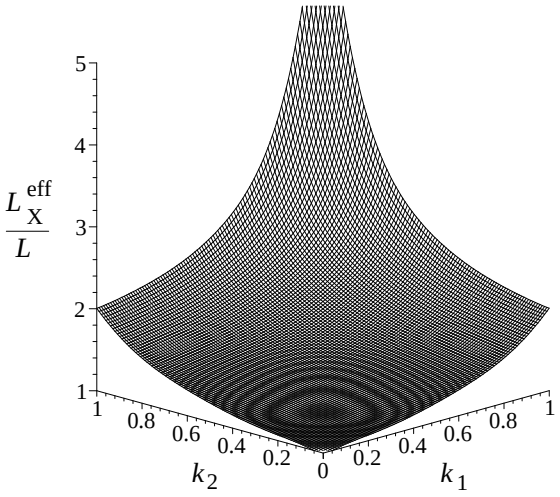

(a) Surface plot

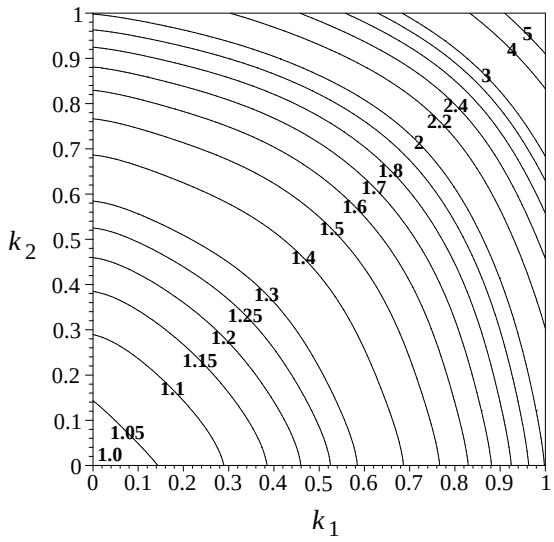

(b) Contour plot

Figure 6.3 Graphical representation of the 7th order polynomial of $L_{\mathrm{X}}^{\mathrm{eff}} / L$ for a column in a rigid-jointed sway frame

6.3 Prediction of the shear strength of reinforced concrete deep beams

6.3.1 Introduction

Reinforced concrete deep beams are common structural elements. They are used for load distribution, for example as transfer girders, pile caps, folded plates and foundation walls, often receiving many small loads and transferring them to a small number of reaction points. They are characterised as being relatively short and deep, having a thickness that is small relative to their span or depth, and being primarily loaded in their own plane.

Due to their geometric proportions, the capacity of reinforced concrete deep beams is governed mainly by shear strength. Despite the large amount of research carried out over the last century, there is no agreed rational procedure to predict the failure mechanism because of its associated complexity. In addition, the design of reinforced concrete deep beams has not yet been covered by BS8110 (1997) which explicitly states that "for the design of deep beams, reference should be made to specialist literature". Comparisons between test results and predictions from other codes, such as ACI (318-95) and CIRIA Guide 2, show poor agreement (Teng et al., 1998).

This application investigates the feasibility of using the GP to predict the shear strength of reinforced concrete deep beams. The GP model will be directly evolved from a set of experimental results available in the literature. A parametric study is

conducted to examine the validity of the GP model predictions outside the range defined for its construction.

6.3.2 Training data

The main parameters influencing the shear strength of reinforced concrete deep beams are the concrete compressive strength, main longitudinal bottom reinforcement, horizontal and vertical web reinforcement, beam width and depth, shear-span and beam-span (Ashour, 2000, Kong et al., 1970, Smith and Vantsiotis, 1982).

Both the shear strength λ and the variables x_1, x_2, x_3, x_4, x_5, and x_6 can be normalised as follows:

- Normalised shear strength: $\lambda = f(x_1, x_2, x_3, x_4, x_5, x_6) = \dfrac{P}{b\, h\, f_c'}$

  where: P = shear failure load,

  b = beam width,

  h = overall beam depth,

  f_c' = concrete compressive strength.

- Shear span to depth ratio: $x_1 = \dfrac{a}{h}$

- Beam span to depth ratio: $x_2 = \dfrac{L}{h}$

- Smeared vertical web reinforcement ratio: $x_3 = \dfrac{A_{sv}\, f_{yv}}{b\, s_v\, f_c'}$

where: A_{sv} = area of vertical web reinforcement,

s_v = horizontal spacing of vertical web reinforcement,

f_{yv} = yield stress of vertical web reinforcement.

- Smeared horizontal web reinforcement ratio: $x_4 = \dfrac{A_{sh}\ f_{yh}}{b\ s_h\ f_c'}$

where: A_{sh} = area of horizontal web reinforcement,

s_h = vertical spacing of horizontal web reinforcement,

f_{yh} = yield stress of horizontal web reinforcement.

- Main longitudinal bottom reinforcement ratio: $x_5 = \dfrac{A_{sb}\ f_{yb}}{b\ h\ f_c'}$

where: A_{sb} = area of main longitudinal bottom reinforcement,

f_{yb} = yield stress of main longitudinal bottom reinforcement.

- Main longitudinal top reinforcement ratio: $x_6 = \dfrac{A_{st}\ f_{yt}}{b\ h\ f_c'}$

where: A_{st} = area of main longitudinal top reinforcement

f_{yt} = yield stress of main longitudinal top reinforcement

Fig. 6.4 shows the geometric dimensions and reinforcement of the deep beam considered in this application.

There is an enormous amount of test results of reinforced concrete deep beams referred to in the literature. Test results of 141 deep beams reported by de Paiva and Siess (1965); Ramakrishnan and Ananthanarayana (1968); Suter and Manuel (1971); Manuel et al. (1971); Kong et al. (1970; 1972); Smith and Vantsiotis (1982); Rogowsky et al. (1986); Subedi et al. (1986; 1988); and Tan and Lu (1999) are used

to create the GP response. The training data set covers a wide range of parameters as given in Table 6.1.

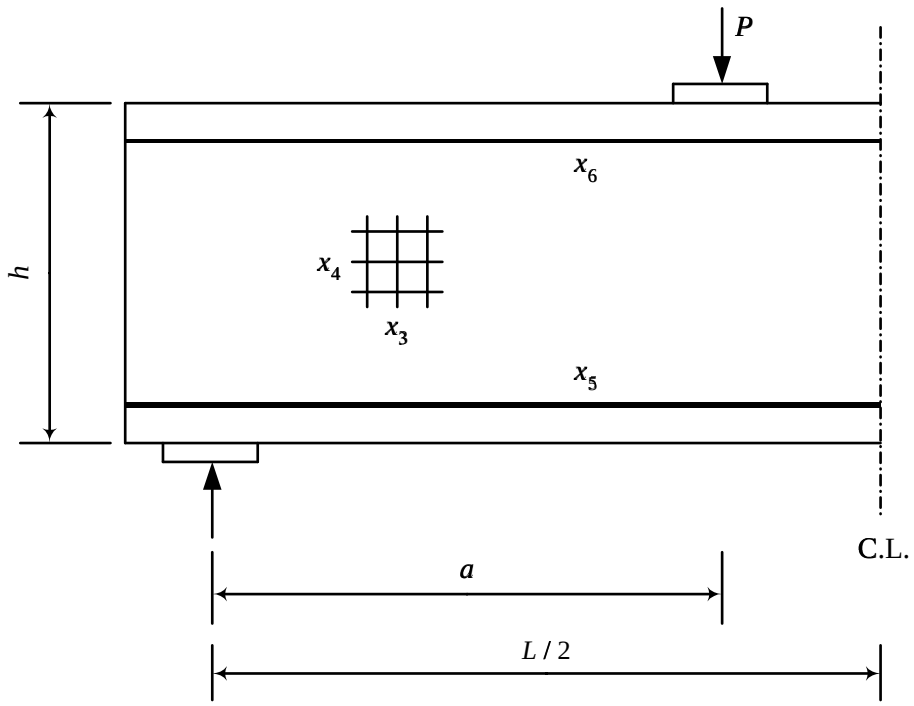

Figure 6.4 Geometrical dimensions of deep beams

Table 6.1 Range of normalised function and parameters in the training data set

	Minimum	**Maximum**
x_1	0.28	2.0
x_2	0.9	4.14
x_3	0.0	0.32
x_4	0.0	0.21
x_5	0.023	0.445
x_6	0	0.128
$\lambda(x_1, x_2, x_3, x_4, x_5, x_6)$	0.029	0.308

6.3.3 GP response

The mathematical operators addition, multiplication, division, square and negation and a population size of 500 individuals were selected in the initial runs. From the beginning, it was observed that variable x_2 had small influence on the shear failure capacity λ and, on one occasion, GP did not include this variable in the evolved expression. It also appeared that variables x_1 and x_5 were the most significant parameters.

In the next stage, only variables x_1, x_3, x_4, x_5 and x_6 were used. Multiple runs were performed and the solutions analysed on the basis of the simplest generated model that conformed as closely as possible with the engineering understanding of the failure mechanism. When the population size was increased to 1000 individuals and the mutation rate set to 0.001, the following model emerged:

$$\lambda = x_5 * (4.31 + 0.15 * x_1^2 + 12.11 * x_1 * x_5 + 3.34 * x_1 * x_6 + 0.66 * x_3 + 0.47 * x_4 + 23.27 * x_5^2 - 16.97 * x^1 * x_5^2 - 18.22 * x_5 - 2.70 * x_1) \quad (6.5)$$

Solutions with better fitness than (6.5) were produced, but they were rejected because of their excessive length. Simplicity is a requirement and, as the complexity of the model increases, its ability to generalise can be affected by the risk of overfitting the data.

The final structure of expression (6.5) was found acceptable, but the coefficients needed to be adjusted in order to satisfy some engineering knowledge

constraints ($\lambda > 0$). A sequential quadratic programming (SQP) algorithm (Madsen and Tingleff, 1990) was applied to produce the final model, as follows:

$$\lambda = x_5 * (3.50 + 0.20 * x_1^2 - 1.76 * x_1 + x_1 * (3.3 * x_5 + 3.37 * x_6 - 1.66 * x_5^2) - 10.67 * x_5 + 9.8 * x_5^2 + 0.63 * x_3 + 0.71 * x_4) \quad (6.6)$$

Expression (6.6) gives an RMS error over the training data of 0.031. The averaged ratio of the shear strength prediction (λ) over the experimental one (λ_e) is $\lambda / \lambda_e = 1.02$, and the standard deviation is equal to 0.22. Figure 6.5 shows a comparison between the experimental and the predicted shear capacity for the training data.

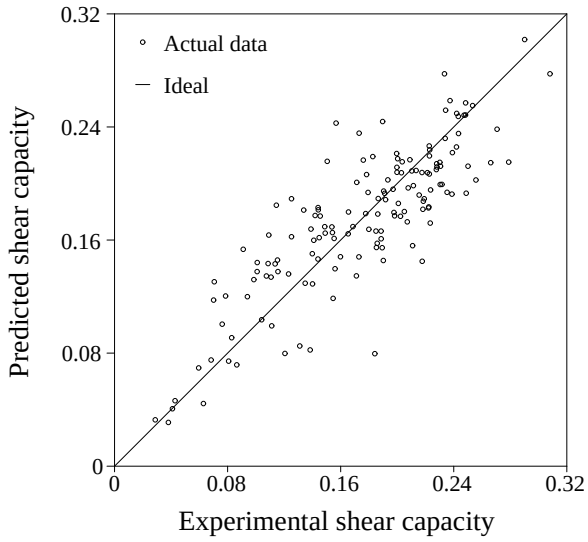

Figure 6.5 Comparison of experimental and predicted shear capacity

To validate the model, 11 additional experimental results were used and detailed in Table 6.2. The RMS error over the validation data is 0.011.

Table 6.2 Validation data set

Reference	x_1	x_3	x_4	x_5	x_6	λ_e	λ	λ / λ_e
De Paiva	0.8889	0.0843	0.0000	0.1413	0.0834	0.2030	0.208	1.023
Kong (1970)	0.5000	0.0855	0.0855	0.1049	0.0256	0.2214	0.208	0.938
Manuel et al.	0.5793	0.0000	0.0000	0.0904	0.0000	0.1542	0.165	1.072
Ramakrishnan	0.3776	0.0334	0.0334	0.0743	0.0000	0.1390	0.168	1.207
Rogowsky	1.6667	0.0000	0.0239	0.1071	0.0064	0.0684	0.075	1.099
Smith& Vantsiotis	0.8571	0.1342	0.1450	0.3519	0.0192	0.2339	0.232	0.992
Subedi et al.	0.9389	0.0626	0.1033	0.1222	0.0475	0.1442	0.181	1.259
Tan and Lu	0.5029	0.0141	0.0141	0.2824	0.0028	0.1568	0.243	1.549
Suter	1.2324	0.0000	0.0000	0.2899	0.0000	0.1190	0.108	0.907
Suter	1.2324	0.0000	0.0000	0.2899	0.0000	0.1590	0.108	0.679
Suter	1.2324	0.0000	0.0000	0.2899	0.0000	0.1640	0.108	0.658
							Average	**1.03**
							Standard deviation	**0.25**

6.3.4 Parametric study

The influence of the two main parameters x_1 and x_5 on the shear strength λ is studied next. In this application, expression (6.6) has been used for prediction of the shear capacity outside the range where the model was constructed. Parameter x_1 is predicted up to the value 2.5 and parameter x_5 starts from the value 0 (see Table 6.1 for initial range).

Figure 6.6 gives the relationship between the shear span to depth ratio x_1 against the shear capacity λ for different values of the normalised main longitudinal

bottom reinforcement x_5 (0.025, 0.05, 0.075, 0.1 and 0.2). A significant reduction on the dimensionless shear capacity λ is observed with the increase of the shear span to depth ratio x_1; this behaviour was experimentally and computationally observed by other researchers (Ashour, 2000, Kong et al., 1970, Smith and Vantsiotis, 1982).

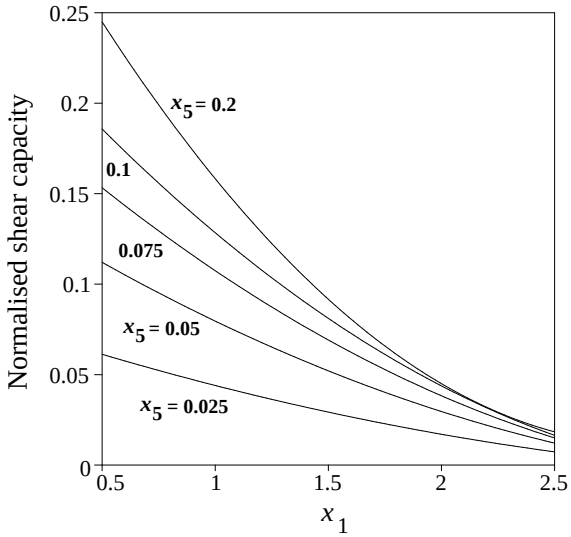

Figure 6.6 Effect of x_1 on the shear strength

The influence of the main longitudinal bottom reinforcement ratio x_5 on the dimensionless shear capacity λ is presented in Figure 6.7 for different shear span to depth ratios x_1 (0.5, 1.0, 1.5, 2.0 and 2.5) and no web reinforcement. For all cases, the dimensionless shear capacity is increasing with the increase of main longitudinal bottom reinforcement. The rate of increase of the shear capacity is reduced with the increase in the main longitudinal reinforcement. These observations agree well with conclusions obtained elsewhere (Ashour, 2000, Kong et al., 1970, Smith and Vantsiotis, 1982).

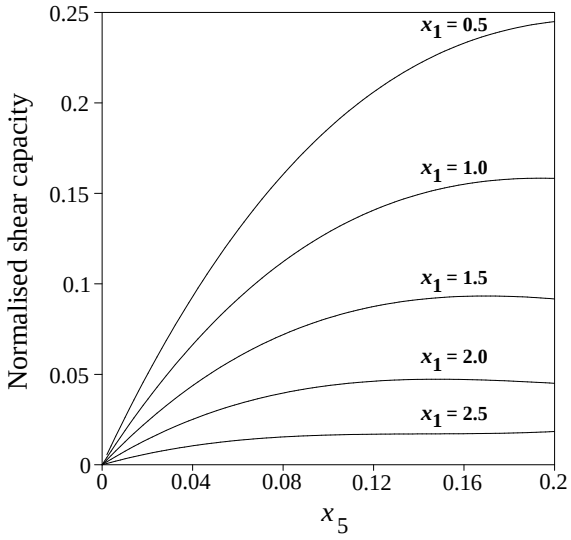

Figure 6.7 Effect of x_5 on the shear strength

6.4 Multicriteria optimization of the calcination of Roman cement

6.4.1 Introduction

In the 19th century, Roman cement was used throughout Europe for the production of stucco finishes in architectural decoration. However, problems with the supply of raw materials and developments in Portland cements motivated the decline in its use and the corresponding loss of craft techniques.

The Charter of Venice (1964) states that the process of restoration should be based on respect for the original material. This is in contrast with the use of the current modern cement products, finishing layers and paints that do not match the original physical and mechanical properties of the stuccoes.

Consequently, for the re-introduction of Roman cement, there is a need to find a suitable range of similar materials among the re-emerging natural hydraulic binders, and to appreciate the technical knowledge and understanding of the original cement-makers. Hughes et al. (1999) have reported experimental results on the calcination of cement-stones from the Harwich and Whitby group of cements. This shows that both setting time and strength development are functions of source and calcination temperature.

In this application, a single source of cement-stone was identified for experimentation within an optimization programme to relate mechanical and mineralogical characteristics to calcination conditions. Genetic programming has been used to illustrate the general trends of minerals and the strength development of

the cement. The data will be useful for the selection of hydraulic binders and as an element in the re-introduction of Roman cement to the European market.

6.4.2 Experimental work

The cement-stones used in this research were collected from the Yorkshire coast at Whitby Long Bight.

The calcination process is not well documented in the historic literature. Previous work at Bradford University has utilised temperatures of 940°C and 1100°C and found the lower temperature to offer better product (Hughes et al., 1999). For the current research, the Audze-Eglais plan of experiments shown in Figure 6.8 has been used with 10 initial and 2 supplementary points. Each cement is referred to using the nomenclature of temperature and residence time, e.g. 917/276 taken as design variables x_1 and x_2 respectively. An electric kiln was used and no attempt made to either circulate air through it or to seal it during calcination. It is therefore to be expected that some cements would be produced under reducing conditions (low oxygen content in the kiln). As more experience is gained of this group of cements, this and additional factors will be added to future optimization programmes.

Ten kilogram batches of raw material underwent an overnight pre-soak at 300°C prior to increasing the temperature. This procedure was introduced in earlier programmes to prevent the explosive disintegration of larger stone fragments in the kiln. The kiln was raised to the required temperature maintained for the specified time and then allowed to cool overnight before the samples were removed for grinding. All cements were ground to <150μm. Characteristics of the cements may

be found in (Hughes et. al., 2000). X-ray diffraction was used to identify mineral phases (e.g. silica, larnite, gehlenite and anhydrite) and the inclusion of boehmite as an internal standard enabled their quantification.

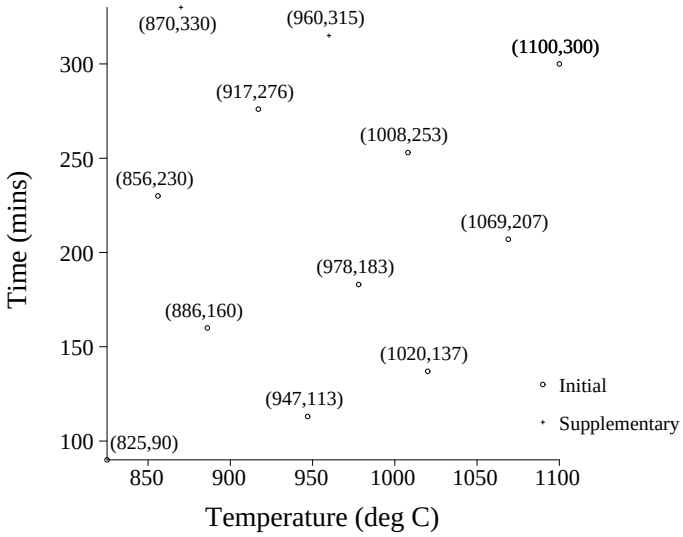

Figure 6.8 Plan of experiments

6.4.3 Results

GP has been used to illustrate the general trends of consumption and production of minerals. For each data set, three possible models were generated and one selected based on the engineering understanding of the calcination process.

In order to describe the intensity of calcination it is convenient to use the terms low, moderate and high. The position of these areas is indicated in Figure 6.9. However, it must be recognized that the zones are not sharply divided but merge into one another.

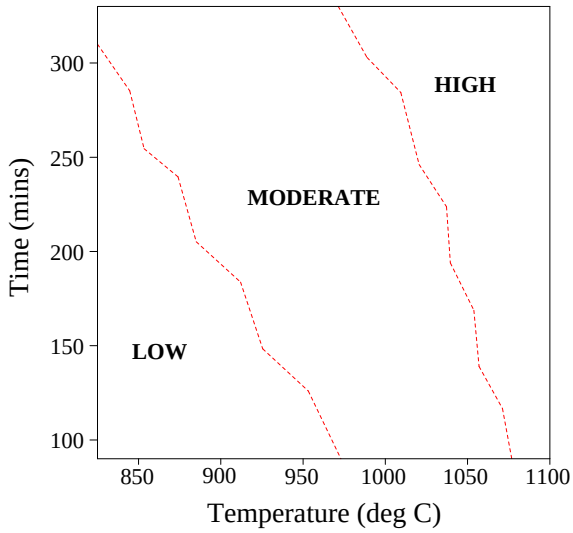

Figure 6.9 Intensity of calcination

Calcite was only detected in cements 825/90, 856/230 and 886/160 and does not provide adequate data for GP manipulation. An alternative presentation of weight loss on calcination (LOC) was used, which may be related to comments found in the historic literature stating that calcination should be "just enough to minimize the weight". Figure 6.10 shows concentration contours for Silica, Larnite, Gehlenite and Anhydrite expressed as relative intensities using the boehmite as a reference. Additionally, LOC contours are expressed as a percentage of the original weight. Caution must be exercised in the interpretation of the data and only the general trends extracted, particularly in the region occupied by cement 825/90 since it is considered to be under-fired to the extent of being unrepresentative.

From the results, it is clear that as the calcination becomes more intense, LOC increases and the unreacted silica decreases with the latter being detected in trace quantities in cements of high calcination. The larnite concentration increases with intensity of calcination, appearing to reach a maximum in the middle of the range.

Whilst gehlenite is always present, its maximum is at a higher intensity of calcination than noted for larnite. Any link between the decrease in larnite and increase in gehlenite must await further investigation.

Figure 6.10 also shows the concentration of anhydrite to be calcination dependent. The decline in anhydrite with more intense calcinations was accompanied by the emergence of Ye'elminite. Cements 825/90, 856/230, 886/160 and 947/113 also show the presence of calcium sulfite, which is associated with reducing conditions. Pastes of these cements turned green when immersed in water, albeit very slight in the case of 947/113 which also only contained a trace of the sulfite.

All cements registered a final setting time much shorter than that of Portland cement, with values in the range 30 seconds to 113 minutes.

Strength development has been determined up to an age of 6 months and 3 broad categories of development identified, which correspond to the 3 intensities of calcination decribed in Figure 6.11. Category 1 is associated with low intensity calcination conditions, category 2 follows moderate calcination and category 3 is displayed following high calcination.

Historically, Roman cements were often compared for quality on the basis of the rapidity of their set, although it should be recognised that the rapid setting times of some of the current pastes are shorter than those prevalent in the 19th century (typically 5-15 minutes).

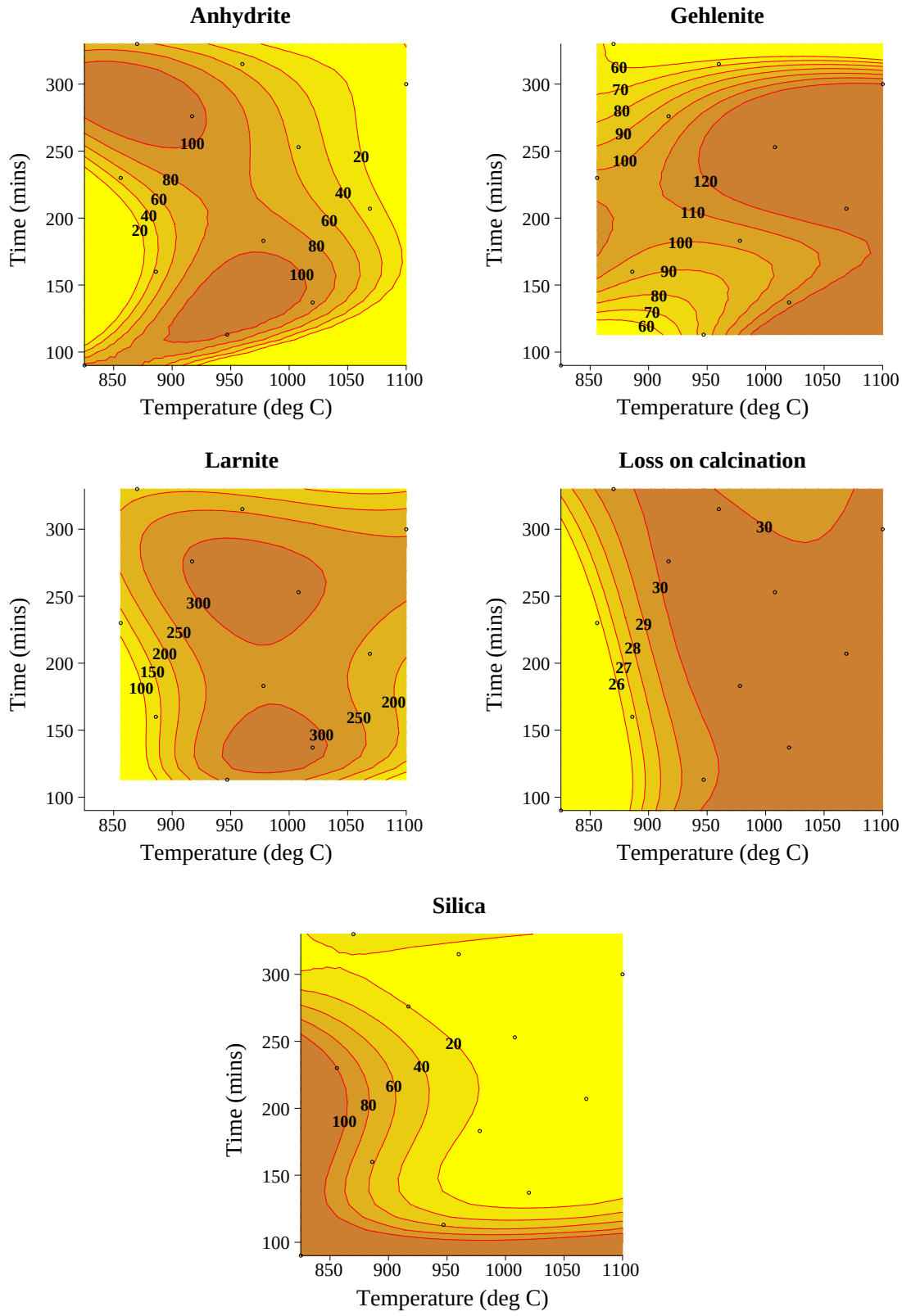

Figure 6.10 Contour plot for principal compounds of Roman cement

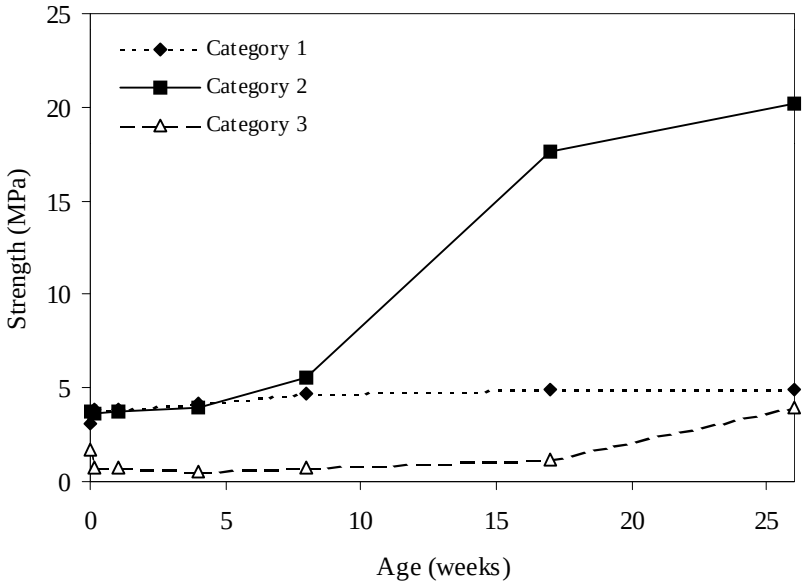

Figure 6.11 Strength development categories

Using GP, contour plots of setting time (minutes), strength at 1 week (Mpa) and rate of strength enhancement between 8 and 17 weeks (MPa/week) have been found and are shown in Figure 6.12. Whilst the most rapid setting and highest early age strength are associated with low-moderate calcinations, the long term strength enhancement results from moderate calcination. Superimposing the contours for larnite concentration and long term rate of strength enhancement produces the unsurprising correlation between the two parameters. The exception is cement 1008/253, although the enhancement appears to be merely delayed, and if determined between 17-26 weeks, it would exhibit a performance similar to the best cement between 8-17 weeks. This behaviour requires further investigation.

The expressions corresponding to all approximations in Figures 6.10 and 6.12 are described in Appendix A.

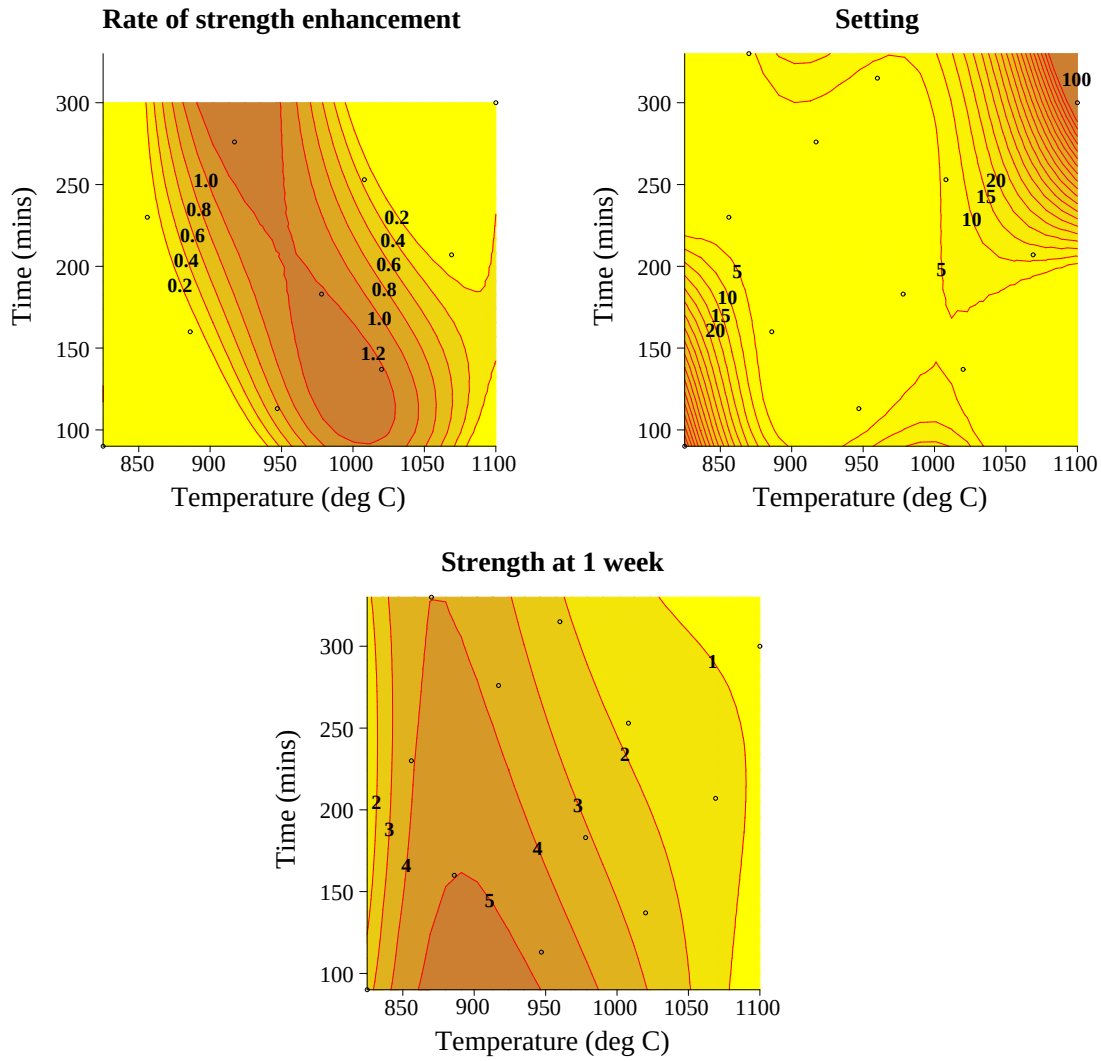

Figure 6.12 Setting time and strength development of Roman cement

6.4.4 Multicriteria optimization

The multicriteria optimization problem is stated as to maximize the early age strength and the rate of strength enhancement simultaneously.

The constraints have been established following different technical aspects. Although the green discolouration of some pastes is associated with the presence of calcium sulfite, its concentration is too low to quantify. Consequently this constraint

has been represented by a maximum silica content (determined by X-ray difraction using boehmite as an internal standard) expressed as relative intensity 50. This correlates with pastes which do not turn green. Further work on the materials aspect of the investigation is required to refine this constraint and provide a direct measure of greenness. The LOC of 28-30% has been selected to represent the confused historic statements of "calcine sufficient to decarbonate", "just enough to minimize the weight" and "underfire to economize on grounding" found in the literature.

The setting time constraint imposes an artificially tight limitation since historical Roman cements which set too rapidly were exposed to the air for a short period of time. A thin layer of cement 917/276 was exposed to the laboratory air for 24 hours and subsequently assessed for setting and strength development. The setting time was increased from 30 seconds to 5 minutes. The early age strength and the rate of strength enhancement was slightly decreased, but still yielded an excellent product.

Knowing that the setting could be controlled naturally, this constraint was removed and the multicriteria optimization problem defined. Table 6.3 shows the formulation of the optimization problem.

Table 6.3 Definition of the optimization problems

Strength at 1 week	$\rightarrow$	*max*
Rate of strength enhancement	$\rightarrow$	*max*
Subject to:		Silica $\leq$ 50
		28% $\leq$ LOC $\leq$ 30%

6.4.5 Pareto-optimal solution set

A characteristic of problems with multiple criteria is that the solutions in the search space are not optimal from the point of view of any single objective, therefore the objective functions are in conflict with one another. A set of solutions must be found such that it is not possible to improve any of them without deteriorating at least one of the other objective functions. These solutions are known as Pareto-optimal solutions. Solutions belonging to the Pareto-optimal set are to be considered by a specialist and a single solution can then be established on the basis of some additional information, e.g. about the relative merits of these criteria or some additional criteria. The choice of one particular solution is a compromise decision that depends on the features of the particular problem and the knowledge of the designer concerning the problem.

A vector $\boldsymbol{x}^*$ is Pareto-optimal if and only if there is no vector $\boldsymbol{x}$ such that

$$\begin{aligned} F_j(\boldsymbol{x}) &\geq F_j(\boldsymbol{x}^*) \qquad \text{for all } j = 1,...,m \\ F_j(\boldsymbol{x}) &> F_j(\boldsymbol{x}^*) \qquad \text{for at least one } j = 1,...,m \end{aligned} \tag{6.7}$$

For all non-Pareto-optimal vectors, the value of at least one objective function F_j can be increased without decreasing the functional values of the other components.

To find the Pareto-optimal set, first the objective and constraint functions have been plotted to identify the feasible solution domain. Second, the numerical solution has been performed by an SQP algorithm (Madsen and Tingleff, 1990) at regular intervals. The final solution is represented in Figure 6.13. The yellow areas define

the feasible solution domains, the red function is the strength at one week, the green function is the rate of strength enhancement and the blue functions are the constraints. The points define the discrete approximation of the Pareto-optimal set.

6.4.6 Discussion of the results of the optimization

The analysis of the optimization (Figure 6.13) reveals that there are three main zones of study according to the obtained Pareto-optimal set: the upper, middle and lower zones.

The lower zone has a very narrow and essentially constant time band. As temperature increases, the strength at one week decreases but the rate of strength enhancement increases. The upper zone has a narrower temperature band than the lower zone. Here as the temperature reduces, the time increases. As this progression is followed, the same trend as before is noted in terms of the strength at 1 week and the rate of strength enhancement. The middle zone is located in a very narrow area of the feasible domain that suggests uncertainty about the validity of these solutions.

It is possible to identify three points that yield similar optimal performance but obtained under different calcination conditions (points A, B, C in Figure 6.13) as described in Table 6.4.

It appears that as the calcination temperature is raised, then the residence time is reduced. The final selection of any of these calcination conditions will be mainly influenced by energy and hence financial and ecological considerations.

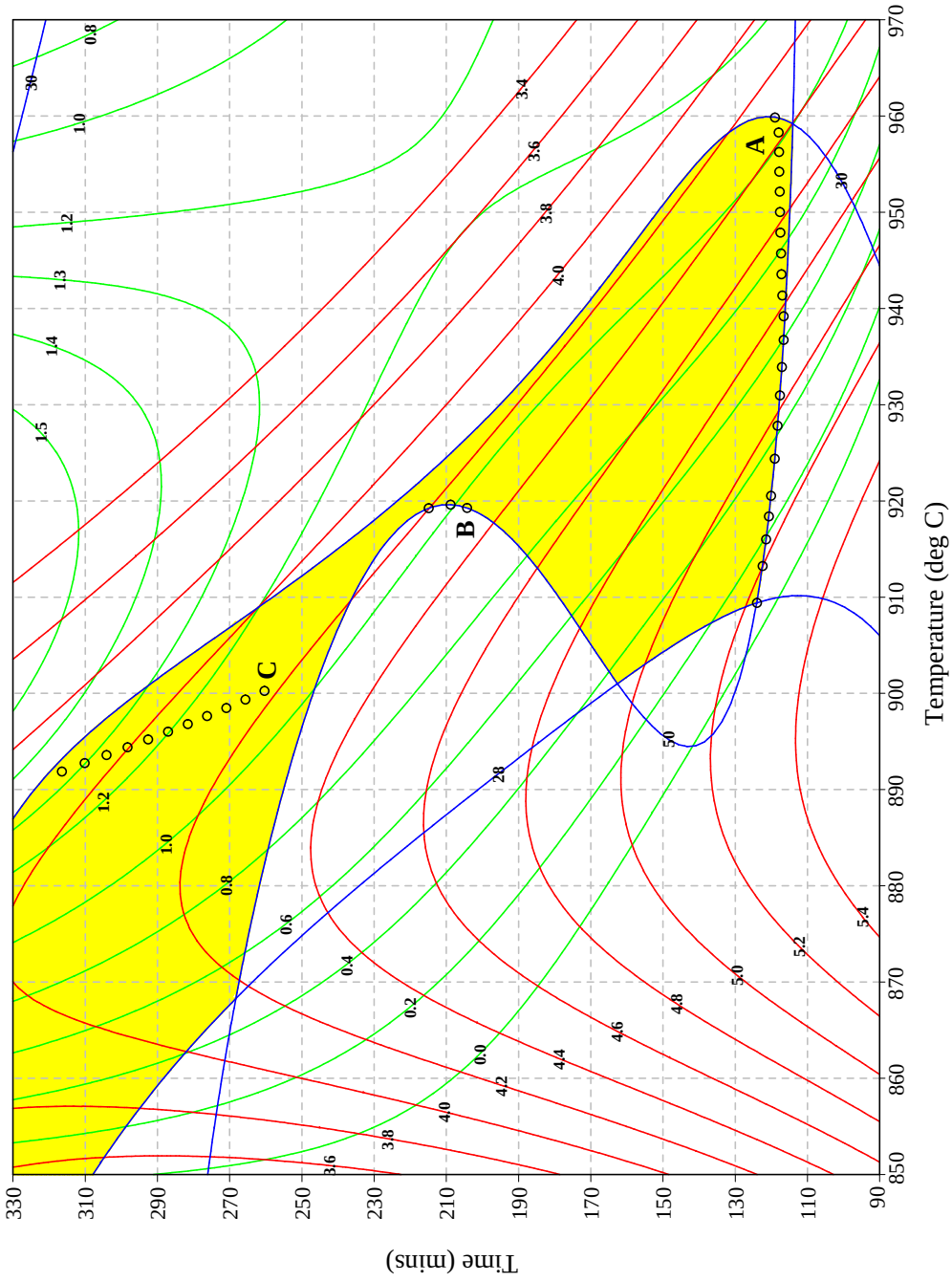

Figure 6.13 Optimization problem and Pareto-optimal solution set

Table 6.4 Solutions from Pareto-optimum set

	Strength at 1 week (MPa)	Rate of strength enhancement (MPa/week)	Temperature (°C)	Time (mins)
A	4.4	1.0	957	120
B	4.3	1.0	920	205
C	4.2	1.1	900	260

6.5 Conclusion

Genetic programming has been successfully applied to approximation building problems with experimental response. Several conclusions can be drawn from the results:

- GP can suggest the structure of the approximate model, but in order to obtain a physically correct and compact analytical expression, it should be guided by the engineering knowledge of the designer.
- GP can predict the response beyond the range of the variables defined in the plan of experiments (e.g. the range was expanded by 25% in example 6.2), although this cannot be generalised for every case.
- GP can detect important variables and reject irrelevant ones (example 6.2).
- GP is a powerful tool for the modelling and optimization of industrial processes (example 6.3).